FIRST-ORDER SYSTEM LEAST SQUARES AND ELECTRICAL IMPEDANCE TOMOGRAPHY: PART II

H. R. MacMILLAN*, T. A. MANTEUFFEL†, AND S. F. McCORMICK†

Abstract. The limited capacity for resolution in Electrical Impedance Tomography (EIT), due to the necessarily finite set of inexact boundary data and the diffusive nature of current flow into the interior, traditionally leads to the conclusion that reconstructing the interior impedance is an ill-posed problem. EIT inherits this difficulty from the simplified inverse problem of reconstructing electrical conductivity, the reciprocal of resistivity. In this study, we begin with the static assumption and consider the reconstruction of conductivity only, leaving that of the impedance as future work. Each functional in the first-order system least-squares (FOSLS) framework, previously established in [10], is proved to be equivalent to a certain measure of error, a metric on the admissible conductivities. With the assumption of complete boundary information, this measure may be considered a norm. Analysis of the topology induced by the norm reveals the qualities of the exact conductivity that one can, in practice, expect to recover. Finally, preliminary numerical results for the FOSLS formulation are shown to be faithful to the presented theory.

1. Introduction. In our companion paper [10], equivalence of three least-squares formulations for Electric Conductivity Tomography (ECT) was established. Implicitly, minimization of a least-squares functional leads to an approximation of the true conductivity that is faithful to the functional's expression of error. Given this perspective, we address the notorious ill-posedness of ECT by deriving a natural norm on conductivity based on the equivalent expressions of error. This enables formulating the inverse problem of ECT as a well-posed elliptic minimization principle. Essentially, the one-to-one correspondence between a conductivity profile and its associated NtD map implies that the operator norm on the space of NtD maps induces a metric on the admissible conductivity. With the assumption of complete boundary data, we show that this metric can be used to construct an equivalent local norm on the defect between conductivities. Ellipticity of the functional in the natural norm implies that, given a Rayleigh-Ritz discretization for conductivity, a unique minimizer is guaranteed in the corresponding topology. Moreover, analysis of this topology leads to an understanding of the components of an exact conductivity that one can and cannot expect to recover. Without complete knowledge of the Neumann-to-Dirichlet (NtD) map, one cannot rely on uniqueness of the inverse problem and therefore cannot expect to establish a definite lower bound. This situation is analogous to the standard finite element solution of elliptic PDE's in that only an inexact representation of the right side is available. The subtlety of this inverse problem is that a discretization of the "image" space is pre-imposed by the choice of finitely many boundary data pairs. We derive an ellipticity result under the assumption of complete boundary information; i.e, uniqueness is assumed so as to allow formally speaking of a "norm" on conductivity. This unrealistic restraint is then relaxed to provide insight into the practical least-squares formulations discussed in our companion paper [10]. The end result is a class of discrete well-posed formulations of ECT.

Our approach represents a significant departure from convention in that we do not rely on a generic regularization term. Rather, we accept and incorporate the underlying physics, albeit inhibiting. Problem-specific information, sometimes used

*Department of Mathematics, Department of Chemistry and Biochemistry, M/C 0365, University of California at San Diego, La Jolla, CA 92093-0365 (hmacmill@mccammon.ucsd.edu). This research was conducted during support from NSF VIGRE grant DMS-9810751.

†Department of Applied Mathematics, Campus Box 526, University of Colorado at Boulder, Boulder, CA 80309-0526 (tmanteuf@colorado.edu, stevem@colorad.edu)

to regularize the ill-posed problem, can be included by either introducing an additional term to the functional or supplementing the space of admissible conductivity.

1.1. Preliminaries. To begin, we recall useful notation and remarks from [10]. Typically, ECT is associated with theNeumann problem

$$\begin{aligned} \nabla \cdot \sigma \nabla p &= 0\,, \\ \mathbf{n} \cdot \sigma \nabla p &= h\,, \end{aligned} \tag{1.1}$$

where the normal current, $h \in \mathrm{H}^{-1/2}(\Gamma)$, satisfies $\int_\Gamma h\, ds = 0$. The coefficient, σ, then determines a "Neumann-to-Dirichlet map."

DEFINITION 1.1. *Denote* $\mathrm{L}^\infty_+(\Omega) := \{\sigma \in \mathrm{L}^\infty(\Omega) : \sigma > 0\}$. *Also, let*

$$\begin{aligned} \mathrm{H}^{1/2}_0(\Gamma) &:= \left\{ g \in \mathrm{H}^{1/2}(\Gamma) : \int_\Gamma g\, d\tau = 0 \right\}, \\ \mathrm{H}^{-1/2}_0(\Gamma) &:= \left\{ h \in \mathrm{H}^{-1/2}(\Gamma) : \int_\Gamma h\, d\tau = 0 \right\}. \end{aligned}$$

A conductivity, $\sigma \in \mathrm{L}^\infty_+(\Omega)$, *defines a bounded linear map,* $\mathcal{R}_\sigma : \mathrm{H}^{-1/2}_0(\Gamma) \longrightarrow \mathrm{H}^{1/2}_0(\Gamma)$, *from the imposed normal current to the resulting boundary voltage. We write*

$$\mathcal{R}_\sigma(h) = p_{|\Gamma}\,,$$

where p solves (1.1), and call $\mathcal{R}_\sigma$ *the Neumann-to-Dirichlet (NtD) map.*

REMARK 1. *The function space,* $\mathrm{L}^\infty_+(\Omega)$, *is used above since it is the least restrictrive space for which the NtD map associated with (1.1) can be defined. However, uniquely defining the NtD may require further restriction, depending upon, as discussed in [10], whether conductivity is continuous or merely piecewise continous. As a matter of convenience, we use* Σ *to denote a function space for which uniqueness has been established. Our aim is thus an analysis of the induced topology on* Σ.

DEFINITION 1.2. *We say that* $\{p, \mathcal{R}_\sigma(h), h\} \in \mathrm{H}^1(\Omega) \times \mathrm{H}^{1/2}_0(\Gamma) \times \mathrm{H}^{-1/2}_0(\Gamma)$ *is a Dirichlet-Neumann triple (DN triple) for* σ *if (1.1) holds. Also, we refer to* $\{\mathcal{R}_\sigma(h), h\}$ *as a DN pair.*

DEFINITION 1.3. *The inverse problem of electrical conductivity tomography (ECT) is to approximate the exact conductivity,* σ^*, *according to a given graph of measured Dirichlet-Neumann data,* $\{g_i, h_i\}_{i=1}^L$, *where* $g_i \approx \mathcal{R}_{\sigma^*}(h_i)$.

Thus, the inverse problem of ECT is to approximately invert the nonlinear mapping from $\sigma \longrightarrow \mathcal{R}_\sigma$. The approximate nature of this inversion is due to the preimposed discreteness of finite data, the inexactness of this data, and the need to choose a discrete approximation space for conductivity.

2. Posing ECT Well. In line with previous studies on the resolution capacity of ECT [5, 8, 11, 13, 14], analysis begins by considering the operator norm of the defect between the two NtD maps respectively associated with the true conductivity, σ^*, and its approximation, σ:

$$\|\mathcal{R}_\sigma - \mathcal{R}_{\sigma^*}\|_{\mathcal{L}(\mathrm{H}^{-1/2}_0(\Gamma), \mathrm{H}^{1/2}_0(\Gamma))} := \sup_{h \in \mathrm{H}^{-1/2}_0(\Gamma)} \frac{\|(\mathcal{R}_\sigma - \mathcal{R}_{\sigma^*})h\|_{1/2,\Gamma}}{\|h\|_{-1/2,\Gamma}}\,. \tag{2.1}$$

Initially, we assume complete knowledge of $\mathcal{R}_{\sigma^*}$ (i.e., complete and exact boundary data) and interpret (2.1) as an expression of error in conductivity, relative to σ^*. This leads to a norm, also relative to σ^*, in which the operator norm in (2.1) is elliptic; that is, there exist positive constants, c_0 and c_1, and a norm, $\|\cdot\|_{\sigma^*}$, such that

$$c_0\|\sigma-\sigma^*\|_{\sigma^*} \leq \|\mathcal{R}_\sigma - \mathcal{R}_{\sigma^*}\|_{\mathcal{L}(\mathrm{H}_0^{-1/2}(\Gamma),\mathrm{H}_0^{1/2}(\Gamma))} \leq c_1\|\sigma-\sigma^*\|_{\sigma^*} \,. \tag{2.2}$$

That this norm is relative to σ^* elicits obvious concerns that we will address.

To summarize the ensuing analysis, ellipticity is achieved by first arriving at an equivalence statement valid for any given pair of Dirichlet and Neumann data. Then, the sup appearing in (2.1) is performed. Hence, in lieu of the sup, the sum of the squares of the defect term appearing in the numerator of (2.1) also preserves equivalence. In this manner, the theory applies to practical formulations within the FOSLS framework. Though the equivalent quantity is then definitely not a metric on the space of admissible conductivity, the bounds do offer insight as to the error, $\sigma-\sigma^*$, that ought to be observable for a given set of boundary data.

2.1. A metric on Σ. The operator norm on the defect in the ND maps, defined in (2.1), is a metric on Σ and we write

$$\begin{aligned} d(\sigma,\sigma^*) &:= \|\mathcal{R}_\sigma - \mathcal{R}_{\sigma^*}\|_{\mathcal{L}(\mathrm{H}_0^{-1/2}(\Gamma),\mathrm{H}_0^{1/2}(\Gamma))} \\ &:= \sup_{h\in \mathrm{H}_0^{-1/2}(\Gamma)} \frac{\|(\mathcal{R}_\sigma - \mathcal{R}_{\sigma^*})h\|_{1/2,\Gamma}}{\|h\|_{-1/2,\Gamma}}. \end{aligned} \tag{2.3}$$

The quantity in (2.3) is certainly symmetric, sub-additive (by the triangle inequality), and definite (by uniqueness of $\sigma^*\in\Sigma$). Given the framework established in [10], an immediate consequence is the equivalence of a sup-norm Kohn and Vogelius functional and a sup-norm FOSLS functional to the above metric (see [10] for details on these formulations). We now focus on analyzing the topology that this metric induces.

Naturally, the metric $d(\sigma,\sigma^*)$ gauges a "distance" between σ and σ^*. Even with complete knowledge of $\mathcal{R}_{\sigma^*}$, minimizing this distance, for σ ranging over whatever discrete space we choose for it, is the best that can be done. Indeed, this distance is closely related to the established concepts of "distinguishability" [8],"visibility" [13, 14], and "inference" [12]. However, previous analysis required linearization and, most importantly, does not establish the explicit lower bound in (2.2).

The $\mathrm{H}^{-1/2}$-norm appearing in (2.3) is defined by taking the sup over all dual pairings. Since a Hilbert space is reflexive (i.e., it is the dual of its dual [6]), we treat the $\mathrm{H}^{1/2}$-norm in the numerator of (2.3) in a similar way to obtain

$$d(\sigma,\sigma^*) = \sup_{h_1,h_2\,\in\, \mathrm{H}_0^{-1/2}(\Gamma)} \frac{|\,\langle h_1,(\mathcal{R}_\sigma - \mathcal{R}_{\sigma^*})h_2\rangle_{0,\Gamma}\,|}{\|h_1\|_{-1/2,\Gamma}\|h_2\|_{-1/2,\Gamma}}\,. \tag{2.4}$$

The next lemma, due to Alessandrini [1], is the first step towards translating the natural metric into a tractable expression of error, $\sigma-\sigma^*$, in the interior. While this lemma is well documented, the perspective we take has not been fully explored.

LEMMA 2.1. *Let $\{p_i^*,\mathcal{R}_{\sigma^*}(h_i),h_i\}$ and $\{p_i,\mathcal{R}_\sigma(h_i),h_i\}$ be DN triples for any $h_i\in\mathrm{H}_0^{-1/2}(\Gamma)$, $i=1,2$. Also, let $\sigma=\sigma^*$ on Γ. Then*

$$d(\sigma,\sigma^*) = \sup_{h_1,h_2\,\in\, \mathrm{H}_0^{-1/2}(\Gamma)} \frac{|\int_\Omega(\sigma^*-\sigma)\nabla p_1^*\cdot\nabla p_2\,dx\,|}{\|h_1\|_{-1/2,\Gamma}\|h_2\|_{-1/2,\Gamma}}\,. \tag{2.5}$$

Proof. Considering the numerator in (2.4), and using the fact that $\sigma = \sigma^*$ on Γ, we have

$$
\begin{aligned}
\langle h_1, (\mathcal{R}_\sigma - \mathcal{R}_{\sigma^*}) h_2 \rangle_\Gamma &= \int_\Omega \nabla \cdot ((p_2 - p_2^*) \sigma^* \nabla p_1^*)\, dx \\
&= \int_\Omega \sigma^* \nabla p_1^* \cdot \nabla (p_2 - p_2^*)\, dx \\
&= \int_\Omega \nabla \cdot (p_1^* \sigma^* \nabla (p_2 - p_2^*))\, dx - \int_\Omega p_1^* \nabla \cdot \sigma^* \nabla (p_2 - p_2^*)\, dx \\
&= -\int_\Omega p_1^* \nabla \cdot \sigma^* \nabla p_2\, dx + \int_\Omega p_1^* \nabla \cdot \sigma \nabla p_2\, dx \\
&= \int_\Omega (\sigma^* - \sigma) \nabla p_1^* \cdot \nabla p_2\, dx\,.
\end{aligned}
$$

□

With modest assumptions regarding the regularity of σ^* and σ, voltages p^* and p are increasingly smooth away from the boundary. Thus the weighting term, $\nabla p_1^* \cdot \nabla p_2$, within the intergral decreases away from the boundary. Alessandrini's result, in this manner, captures natural obscuration of error into the interior. However, it is not clear how to garner explicit insight from (2.5). To further this analysis, we now show that metric $d(\sigma, \sigma^*)$ is equivalent to a "local" norm on Σ.

2.2. A local norm. DEFINITION 2.2. *Relative to a fixed $\sigma^* \in \Sigma$, define the norm*

$$
\|\delta\|_{\sigma^*} := \sup_{h_1, h_2 \,\in\, \mathrm{H}_0^{-1/2}(\Gamma)} \frac{\left|\int_\Omega \delta\, \nabla p_1^* \cdot \nabla p_2^*\, dx\right|}{\|h_1\|_{-1/2,\Gamma} \|h_2\|_{-1/2,\Gamma}}\,, \tag{2.6}
$$

where the sup *is taken over all DN triples, $\{p_1^*, \mathcal{R}_{\sigma^*}(h_1), h_1\}$ and $\{p_2^*, \mathcal{R}_{\sigma^*}(h_2), h_2\}$, associated with σ^*.*

To see that this is indeed a norm, note that $\|\delta\|_{\sigma^*} \geq 0$ and $\|\lambda\delta\|_{\sigma^*} = |\ \lambda\ |\ \|\delta\|_{\sigma^*}$ for any scalar λ. The triangle inequality is also straightforward:

$$
\begin{aligned}
\|\delta + \epsilon\|_{\sigma^*} &= \sup_{h_1, h_2 \,\in\, \mathrm{H}_0^{-1/2}(\Gamma)} \frac{\left|\int_\Omega (\delta + \epsilon)\, \nabla p_1^* \cdot \nabla p_2^*\, dx\right|}{\|h_1\|_{-1/2,\Gamma} \|h_2\|_{-1/2,\Gamma}}\,, \\
&\leq \sup_{h_1, h_2 \,\in\, \mathrm{H}_0^{-1/2}(\Gamma)} \left\{ \frac{\left|\int_\Omega \delta\, \nabla p_1^* \cdot \nabla p_2^*\, dx\right|}{\|h_1\|_{-1/2,\Gamma} \|h_2\|_{-1/2,\Gamma}} + \frac{\left|\int_\Omega \epsilon\, \nabla p_1^* \cdot \nabla p_2^*\, dx\right|}{\|h_1\|_{-1/2,\Gamma} \|h_2\|_{-1/2,\Gamma}} \right\}, \\
&\leq \|\delta\|_{\sigma^*} + \|\epsilon\|_{\sigma^*}
\end{aligned} \tag{2.7}
$$

Finally, definiteness follows from uniqueness of the inverse problem for $\sigma^* \in \Sigma$, once we establish the local norm as an upper bound on (2.1).

Given that $\sigma > 0$, we cannot speak of Σ as a normed linear space with norm (2.6) since it is not a linear space. However, this physical restriction can be suspended so that, only when $\delta(x) > -\sigma^*(x)$, $\forall\, x \in \Omega$, will the norm hold significance for ECT.

The norm defined in (2.6) is a familiar quantity in the literature, arising from the linearization discussed in [10]. However, we do not resort to linearization to derive the significance of this quantity, and we introduce the perspective that (2.6) is in fact the natural norm in which ECT can be posed well. Moreover, the following theorem, which establishes coercivity, is new.

THEOREM 2.3. *Let $\{p_i^*, \mathcal{R}_{\sigma^*}(h_i), h_i\}$, $i = 1, 2$, be DN triples for σ^*. Also, suppose $\sigma = \sigma^*$ on the boundary Γ. If we define a "multiplicative" error $\eta := \frac{\sigma^*}{\sigma} > 0$, then metric (2.3) is locally elliptic in the sense that*

$$(\min_\Omega \eta)\|\sigma - \sigma^*\|_{\sigma^*} \leq d(\sigma, \sigma^*) \leq (\max_\Omega \eta)\|\sigma - \sigma^*\|_{\sigma^*}, \tag{2.8}$$

where

$$\|\sigma - \sigma^*\|_{\sigma^*} := \sup_{h_1, h_2 \in \mathrm{H}_0^{-1/2}(\Gamma)} \frac{\left|\int_\Omega (\sigma - \sigma^*)\, \nabla p_1^* \cdot \nabla p_2^* dx\right|}{\|h_1\|_{-1/2,\Gamma}\|h_2\|_{-1/2,\Gamma}} \tag{2.9}$$

and where the sup *is taken over all DN triples, $\{p_1^*, \mathcal{R}_{\sigma^*}(h_1), h_1\}$ and $\{p_2^*, \mathcal{R}_{\sigma^*}(h_2), h_2\}$.*

Proof. The proof begins by recalling that

$$d(\sigma, \sigma^*) = \sup_{h_1, h_2 \in \mathrm{H}_0^{-1/2}(\Gamma)} \frac{|\langle h_1, (\mathcal{R}_\sigma - \mathcal{R}_{\sigma^*})h_2\rangle_{0,\Gamma}|}{\|h_1\|_{-1/2,\Gamma}\|h_2\|_{-1/2,\Gamma}}. \tag{2.10}$$

From the second line in the proof of Lemma 2.1, we have

$$\langle h_1, (\mathcal{R}_\sigma - \mathcal{R}_{\sigma^*})h_2\rangle_{0,\Gamma} = \int_\Omega \sigma^* \nabla p_1^* \cdot \nabla(p_2 - p_2^*)\, dx,$$

where $\{p_i^*, \mathcal{R}_{\sigma^*}(h_i), h_i\}$ and $\{p_i, \mathcal{R}_\sigma(h_i), h_i\}$, $i = 1, 2$, are DN triples for σ^* and σ, respectively. Hence, for any $h_1, h_2 \in \mathrm{H}_0^{-1/2}(\Gamma)$, the numerator in (2.10) satisfies

$$\begin{aligned}(\min_\Omega \eta) &\left|\int_\Omega \frac{\sigma^*}{\eta} \nabla(p_2 - p_2^*) \cdot \nabla p_1^*\, dx\right| \\ &\leq |\langle h_1, (\mathcal{R}_\sigma - \mathcal{R}_{\sigma^*})h_2\rangle_{0,\Gamma}| \\ &\leq (\max_\Omega \eta)\left|\int_\Omega \frac{\sigma^*}{\eta}\nabla(p_2 - p_2^*) \cdot \nabla p_1^*\, dx\right|,\end{aligned} \tag{2.11}$$

where $\eta := \frac{\sigma^*}{\sigma}$. Next, given that $\sigma = \frac{\sigma^*}{\eta}$ in (2.11), we examine the term

$$\int_\Omega \sigma \nabla p_1^* \cdot \nabla(p_2 - p_2^*).$$

To rewrite this quantity, first observe that

$$\nabla \cdot \sigma \nabla(p_2 - p_2^*) = -\nabla \cdot \sigma \nabla p_2^* = \nabla \cdot (\sigma^* - \sigma)\nabla p_2^*.$$

Then, taking the inner product with p_1^*, integrating by parts, and using the information on the boundary, we find that

$$\int_\Omega \sigma \nabla p_1^* \cdot \nabla(p_2 - p_2^*)\, dx = \int_\Omega (\sigma^* - \sigma)\nabla p_1^* \cdot \nabla p_2^*\, dx. \tag{2.12}$$

Using (2.12) to rewrite (2.11), we have

$$\begin{aligned}(\min_\Omega \eta) &\left|\int_\Omega (\sigma^* - \sigma)\nabla p_1^* \cdot \nabla p_2^*\, dx\right| \\ &\leq |\langle h_1, (\mathcal{R}_\sigma - \mathcal{R}_{\sigma^*})h_2\rangle_{0,\Gamma}| \\ &\leq (\max_\Omega \eta)\left|\int_\Omega (\sigma^* - \sigma)\nabla p_1^* \cdot \nabla p_2^*\, dx\right|.\end{aligned} \tag{2.13}$$

Finally, scaling and taking the sup over all DN triples according to (2.9) proves the theorem. □

Note that the statement of ellipticity in Theorem 2.3 is local in two fundamental respects: the actual norm depends on σ^* and the constants depend directly on σ and σ^*. The dependence of the norm on σ^* means that the upper and lower bounds are not computable. To address this concern, we can simply rearrange the method by which we arrive at these bounds by exchanging the roles of the approximate and unknown quantities. Then, analogous to (2.13), the result is that, for any $h_1, h_2 \in \mathrm{H}_0^{-1/2}(\Gamma)$,

$$
\begin{aligned}
(\min_{\Omega} 1/\eta) \left| \int_{\Omega} (\sigma^* - \sigma) \nabla p_1 \cdot \nabla p_2 \, dx \right| & \\
\leq |\langle h_1, (\mathcal{R}_\sigma - \mathcal{R}_{\sigma^*}) h_2 \rangle_{0,\Gamma}| & \\
\leq (\max_{\Omega} 1/\eta) \left| \int_{\Omega} (\sigma^* - \sigma) \nabla p_1 \cdot \nabla p_2 \, dx \right| . & \qquad (2.14)
\end{aligned}
$$

From this statement, it will follow that we may use p's associated with an approximate conductivity to naturally weight conductivity error away from the boundary. This leads to a computable lower bound that indicates whether a given component of error can be detected. Certainly, prior knowledge of σ^* incorporated into approximation σ provides a more accurate natural weighting in the integrals above.

The second local aspect of the ellipticity result is the presence of the global min and max of $\eta = \frac{\sigma^*}{\sigma}$ as the respective constants in (2.8). In particular, there is an inherent dependence on a priori estimation of σ^*. Yet, we cannot expect to obtain a result independent of both σ and σ^*; e.g., one cannot expect to determine the conductivity within a hollow lead box. It is important to note that the presence of η does not mean that expecting meaningful bounds is tantamount to assuming a regime in which a linearization is valid. For example, consisider a scenario in which several different compartments of different but known conductivities are to resolved spatially. The η terms are known and remain unchanged for estimates associated with various distributions of the internal compartments.

In the language of Backus-Gilbert theory, the equivalent quantity in the above theorem is the maximum singular value of the “response measure” or “Frechet kernel” of the NtD map [11]. The same quantity, independently appearing in Calderon's analysis [4], is known as the “sensitivity matrix” within biomedical literature. However, no explicit lower bound, such as appears in (2.8), is shown in the literature. Moreover, it is remarkable that our ellipticity result is achieved without an explicit linearization and that the multiplicative error, η, appears so concisely.

In Theorem 2.3, restriction to $\sigma \in \Sigma$ merely serves to guarantee definiteness, which validates speaking of a “metric” and of a “norm” on conductivity. Along with relaxing the assumption of complete boundary information, we may relax the admissible space of conductivity to $\sigma \in \mathrm{L}_+^\infty(\Omega)$. This is evident since (2.14) holds so long as $\mathcal{R}_\sigma$ and $\mathcal{R}_{\sigma^*}$ are defined and the integral exists.

2.3. Guided discretization. To this point, complete knowledge of the NtD map has been assumed. Of course, in practice, we have only finite knowledge of boundary data. Exploring the implications of our theory on practical formulations of ECT entails addressing two distinct issues. The first is the limited resolution due to the physics, described by the natural norm defined in the previous section. The second issue is the inaccuracy and pre-imposed discreteness of realistic information on the boundary. The essential question to address is: Given a set of applied Neumann data and a tolerance on the error in the resulting measured Dirichlet data, what components of the error can we expect to reduce, and to what extent? To answer this question is to understand the delicate "trade-off" between resolution and accuracy, the goal of Backus and Gilbert theory [11].

2.3.1. Computable coercive bound. We now present a coercivity result that accounts for the pre-imposed discreteness of the data and sets the stage for addressing the effects of inaccuracy of this data. Given a finite set of boundary data, we wish to determine its capacity to signal a fixed error. Naturally, our result in turn depends on the capacity, using the given span of tests, to interpolate an element of $\mathrm{H}_0^{-1/2}(\Gamma)$ that attains the operator norm of the defect in the NtD maps; i.e., a test that attains

$$\|\mathcal{R}_\sigma - \mathcal{R}_{\sigma^*}\|_{\mathcal{L}(\mathrm{H}_0^{-1/2}(\Gamma),\mathrm{H}_0^{1/2}(\Gamma))} := \sup_{h\in \mathrm{H}_0^{-1/2}(\Gamma)} \frac{\|(\mathcal{R}_\sigma - \mathcal{R}_{\sigma^*})h\|_{1/2,\Gamma}}{\|h\|_{-1/2,\Gamma}}. \qquad (2.15)$$

Note that this test is not necessarily unique. In the remainder of this section, h^* refers to such a test, normalized so that $\|h^*\|_{-1/2,\Gamma} = 1$. We have the following result.

THEOREM 2.4. *Let $\mathcal{T} := Span\{h_i\}_{i=1}^L$ and $\eta := \frac{\sigma^*}{\sigma}$. Also, define $h^* \in \mathrm{H}_0^{-1/2}(\Gamma)$ such that*

$$\|\mathcal{R}_\sigma(h^*) - \mathcal{R}_{\sigma^*}(h^*)\|_{1/2,\Gamma} = \|\mathcal{R}_\sigma - \mathcal{R}_{\sigma^*}\|_{\mathcal{L}(\mathrm{H}_0^{-1/2}(\Gamma),\mathrm{H}_0^{1/2}(\Gamma))}.$$

Then, for any $\phi \in \mathcal{T}$,

$$\begin{aligned}&\|\mathcal{R}_\sigma(\phi) - \mathcal{R}_{\sigma^*}(\phi)\|_{1/2,\Gamma} + c\|h^* - \phi\|_{-1/2,\Gamma} \\ &\qquad\geq (\min_\Omega 1/\eta) \sup_{\psi_1,\psi_2\in\mathcal{T}} \frac{\left|\int_\Omega (\sigma - \sigma^*)\,\nabla p_1\cdot\nabla p_2\,dx\right|}{\|\psi_1\|_{-1/2,\Gamma}\|\psi_2\|_{-1/2,\Gamma}}, \qquad (2.16)\end{aligned}$$

where the sup *is taken over all DN triples, $\{p_1, \mathcal{R}_\sigma(\psi_1), \psi_1\}$ and $\{p_2, \mathcal{R}_\sigma(\psi_2), \psi_2\}$ with $\psi_i \in \mathcal{T}$ and $c = 2\max\{\|\mathcal{R}_\sigma\|_{\mathcal{L}}, \|\mathcal{R}_{\sigma^*}\|_{\mathcal{L}}\}$.*

Proof. For any $h \in \mathrm{H}_0^{-1/2}(\Gamma)$ and $\phi \in \mathcal{T}$, we have that

$$\begin{aligned}\|\mathcal{R}_\sigma(h) - \mathcal{R}_{\sigma^*}(h)\|_{1/2,\Gamma} &\leq \|\mathcal{R}_\sigma(h) - \mathcal{R}_\sigma(\phi)\|_{1/2,\Gamma} + \|\mathcal{R}_{\sigma^*}(h) - \mathcal{R}_{\sigma^*}(\phi)\|_{1/2,\Gamma} \\ &\quad + \|\mathcal{R}_\sigma(\phi) - \mathcal{R}_{\sigma^*}(\phi)\|_{1/2,\Gamma} \\ &\leq c\|h-\phi\|_{-1/2,\Gamma} + \|\mathcal{R}_\sigma(\phi) - \mathcal{R}_{\sigma^*}(\phi)\|_{1/2,\Gamma}, \qquad (2.17)\end{aligned}$$

where $c = 2\max\{\|\mathcal{R}_\sigma\|_{\mathcal{L}}, \|\mathcal{R}_{\sigma^*}\|_{\mathcal{L}}\}$. We may thus write

$$\begin{aligned}&\|\mathcal{R}_\sigma(\phi) - \mathcal{R}_{\sigma^*}(\phi)\|_{1/2,\Gamma} + c\|h^* - \phi\|_{-1/2,\Gamma} \\ &\qquad\geq \|\mathcal{R}_\sigma(h^*) - \mathcal{R}_{\sigma^*}(h^*)\|_{1/2,\Gamma} \\ &\qquad= \sup_{h_1,h_2\in \mathrm{H}_0^{-1/2}(\Gamma)} \frac{|\langle \mathcal{R}_\sigma(h_1) - \mathcal{R}_{\sigma^*}(h_1), h_2\rangle_{0,\Gamma}|}{\|h_1\|_{-1/2,\Gamma}\|h_2\|_{-1/2,\Gamma}}. \qquad (2.18)\end{aligned}$$

Now, using the lower bound in (2.14), we have

$$\begin{aligned}&\|\mathcal{R}_\sigma(\phi) - \mathcal{R}_{\sigma^*}(\phi)\|_{1/2,\Gamma} + c\|h^* - \phi\|_{-1/2,\Gamma} \\ &\qquad\geq (\min_\Omega 1/\eta) \sup_{h_1,h_2\in \mathrm{H}_0^{-1/2}(\Gamma)} \frac{\left|\int_\Omega (\sigma - \sigma^*)\,\nabla p_1\cdot\nabla p_2\,dx\right|}{\|h_1\|_{-1/2,\Gamma}\|h_2\|_{-1/2,\Gamma}}.\end{aligned}$$

Finally,

$$\|\mathcal{R}_\sigma(\phi) - \mathcal{R}_{\sigma^*}(\phi)\|_{1/2,\Gamma} + c\|h^* - \phi\|_{-1/2,\Gamma} \geq (\min_\Omega 1/\eta) \sup_{\psi_1,\psi_2\in\mathcal{T}} \frac{\left|\int_\Omega (\sigma - \sigma^*)\,\nabla p_1 \cdot \nabla p_2\, dx\right|}{\|\psi_1\|_{-1/2,\Gamma}\|\psi_2\|_{-1/2,\Gamma}},$$

restricting the space over which the sup is conducted to DN triples $\{p_1, \mathcal{R}_\sigma(\psi_1), \psi_1\}$ and $\{p_2, \mathcal{R}_\sigma(\psi_2), \psi_2\}$ for $\psi_i \in \mathcal{T}$. □

According to this theorem, applying h^* to the boundary is the best way to signal the error associated with the approximate conductivity. It is natural to choose $\phi \in \mathcal{T}$ as the best approximation to h^* in the $\mathrm{H}^{-1/2}$-norm. Recall that h^* can be approximated without knowledge of σ^* and that, by so targeting the testing, the number of forward problems at each iteration may be reduced [7]. Theorem 2.4 leads to the following corollary to account for error in the measured data $\{g_i\}_{i=1}^L$.

COROLLARY 2.5. *Let h^*, ϕ, and $\mathcal{T}$ be as defined in Theorem 2.4. Also, let $\phi = \sum_i \alpha_i h_i$, where $\{h_i\}_{i=1}^L$ is a basis for $\mathcal{T}$. Finally, define $g_\phi := \sum_i \alpha_i g_i$ to be the measured Dirichlet data associated with ϕ. Then*

$$\|\mathcal{R}_\sigma(\phi) - g_\phi\|_{1/2,\Gamma} + \|g_\phi - \mathcal{R}_{\sigma^*}(\phi)\|_{1/2,\Gamma} + c\|h^* - \phi\|_{-1/2,\Gamma} \geq (\min_\Omega 1/\eta) \sup_{\psi_1,\psi_2\in\mathcal{T}} \frac{\left|\int_\Omega (\sigma - \sigma^*)\,\nabla p_1 \cdot \nabla p_2\, dx\right|}{\|\psi_1\|_{-1/2,\Gamma}\|\psi_2\|_{-1/2,\Gamma}}, \tag{2.19}$$

where $c = 2\max\{\|\mathcal{R}_\sigma\|_\mathcal{L}, \|\mathcal{R}_{\sigma^*}\|_\mathcal{L}\}$ and, again, the sup *is taken over all DN triples, $\{p_1, \mathcal{R}_\sigma(\psi_1), \psi_1\}$ and $\{p_2, \mathcal{R}_\sigma(\psi_2), \psi_2\}$.*

Proof. The proof follows immediately from usingTheorem 2.4 and the triangle inequality to write

$$\|\mathcal{R}_\sigma(\phi) - g_\phi + g_\phi - \mathcal{R}_{\sigma^*}(\phi)\|_{1/2,\Gamma} \leq \|\mathcal{R}_\sigma(\phi) - g_\phi\|_{1/2,\Gamma} + \|g_\phi - \mathcal{R}_{\sigma^*}(\phi)\|_{1/2,\Gamma}.$$

□

The above corollary is the ultimate statement of the theory, accounting for both the pre-imposed discreteness and the potential inaccuracy of the boundary data as they combine to reduce our ability to detect error in the conductivity. Note that the result holds for σ, $\sigma^* \in \mathrm{L}_+^\infty(\Omega)$, the most general space for which the Neumman problem, and thus a NtD map, is defined. For a chosen $\mathcal{T}$ and for ϕ that minimizes $||h^* - \phi||_{-1/2}$ one is left with only the possibility to reduce the first term in (2.19). For a given error, $\sigma - \sigma^*$, the lower bound is computable as the maximum singular value of the sensitivity matrix associated with the span of tests on the boundary. Hence, given an estimate for $c\|h^* - \phi\|_{-1/2,\Gamma}$ and a tolerance on boundary data error term $\|g_\phi - \mathcal{R}_{\sigma^*}(\phi)\|_{1/2,\Gamma}$, a threshold, $\tau > 0$, can be determined so that error $\kappa \cdot (\sigma - \sigma^*)$ cannot be signaled when $|\kappa| < \tau$. We stress that this threshold is relative to the particular error, $\sigma - \sigma^*$. This scale indeterminacy explicitly reveals the compromise, discussed by Parker [12], that must be made when choosing a suitable discretization. On one hand, a basis for $\sigma - \sigma^*$ must be chosen while, on the other, each element in this basis corresponds to a threshold, τ. In the absence of a priori information about the exact conductivity, it is natural to choose a basis corresponding to a single fixed threshold, and consider this a σ-uniform discretization. This is in direct analogy to solving a forward problem, for example Poisson's equation, in that the discretization we propose is one that is uniform relative to the norm in which we can naturally measure error, thus uniformly balancing the cost of reducing such components of a given error.

2.3.2. Basis Constraints. To demonstrate our principle, we use a trigonometric basis for the boundary tests. This enables us to compute the $\mathrm{H}^{-1/2}$-norms analytically, using Fourier transforms [9]. We also consider, as the unknown conductivity, piecewise constant perturbations of a known constant background conductivity. Each cell in the discretizations shown in Figure 2.1 represents the supports of characteristic functions chosen as the basis elements to represent error. To focus attention on fewer degrees of freedom, we require that the average arc of each support is roughly equivalent to the radial dimension, and set the angular orientation of each support arbitrarily. The radial dimensions of the supports are determined so that a constant unit ($\tau = 1$) perturbation results in the same value of the lower bound in (2.19) for each support. Setting this value equal to an estimate of the sum of the second and third terms in (2.19) determines a given discretization. We denote this sum as

$$\epsilon = \|g_\phi - \mathcal{R}_{\sigma^*}(\phi)\|_{1/2,\Gamma} + c\|h^* - \phi\|_{-1/2,\Gamma}$$

and observe, in Figure 2.1, the effect on resolution when we loosen the tolerance from $\epsilon = .1$ to $\epsilon = .2$. Choosing characteristic functions as perturbations, we sacrifice the

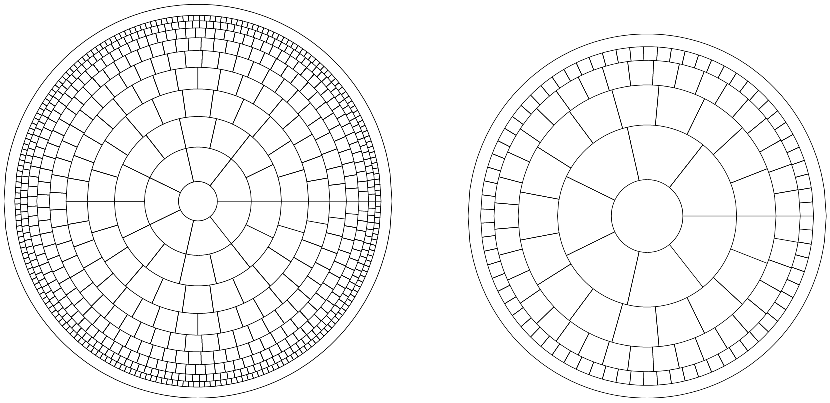

FIG. 2.1. *Two examples of a graded grid: $\epsilon = .1$ and $\epsilon = .2$.*

elimination of perturbations of magnitude less than one. If this is not appropriate, a smaller threshold should be chosen, resulting in a more coarse discretization. However, clearly such practical decisions should be made given insight about the unknown solution. This is a recurring theme in our analysis: it may be readily improved given problem specific information. We therefore stress that the goal of this study is to establish a robust framework into which such insight is easily incorporated.

It is evident that two positive perturbations on either grid illustrated in Figure 2.1 are signaled more loudly than either would be by itself. However, nothing can be said regarding oscillatory error given the chosen space of admissible conductivity. Certainly, the assumption of piecewise constant error is merely the first step in quantifying those errors that can be signaled. Nonetheless, the grids depicted in Figure 2.1 are instructive examples of a sound computational strategy.

Without prior information concerning the nature of the unknown conductivity, the only process governing the discretization is the σ-uniform distribution of error components. As such, a significant amount of arbitrary assumptions contributed to the above example, limiting its scope. Given the inherent restrictions on ECT, it is quite clear that its usefulness as an imaging method may be limited to situations where significant prior information is available. In particular, this information may be structural. In such applications, basis constraints may be imposed to specifically design the space of admissible conductivities. For example, if an application affords placing sole focus on particular regions in a domain, an adequate representation of the unknown conductivity may be achieved with relatively few degrees of freedom. Our established coercivity bound can be used to meaningfully estimate the extent to which error, manifested by such a constrained basis, can be eliminated. Exploring the application of our theory to basis constraints leads to a better understanding of what can be achieved in the presence of problem specific information.

In the following section, we report on the FOSLS functional minimization that we perform. We do not directly appeal to the above mentioned discretization strategy since, as is observed in [10], the FOSLS functional implicitly incorporates the notion of the graded grid in a natural sense.

3. FOSLS minimization. In this section, we review the 2D FOSLS formulation and present preliminary numerical results that are faithful to the above theoretical results. We do not yet bring to full maturation an algorithm that incorporates potentially important components of an efficient multilevel solution, such as *a priori* information and adaptive testing. As such, a full comparison of the examples we present to those existing in the literature is premature. Furthermore, such comparison obscures the fact that our theory concerning the resolution capacity of ECT encompasses not only the FOSLS functional, but also Output Least Squares and the Kohn and Vogelius formulation. Here we discuss these issues and suggest several ways our own algorithm may be streamlined in accordance with the theory.

3.1. Review of FOSLS Formulation. To derive the FOSLS formulation for ECT, define $q := \frac{1}{2}\log(\sigma)$, so that $e^{2q} := \sigma$, and let $\mathbf{u} := e^{q}\nabla p$. Then, with $\{p, \mathcal{R}_\sigma(h), h\}$ a DN triple for σ, consider the first-order system

$$\begin{aligned} e^{-q}\nabla\cdot e^{q}\mathbf{u} &= 0 && \text{in } \Omega\,,\\ e^{q}\nabla\times e^{-q}\mathbf{u} &= 0 && \text{in } \Omega\,,\\ \mathbf{n}\cdot e^{q}\mathbf{u} &= h && \text{on } \Gamma\,. \end{aligned} \tag{3.1}$$

Hence, (3.1) determines the tangential current

$$\mathbf{n}\times e^{-q}\mathbf{u} = (\mathbf{n}\times\nabla)\mathcal{R}_\sigma(h) \in (\mathrm{H}_0^{-1/2}(\Gamma))^{n-1}\,,$$

and thus a normal-to-tangential (NtT) map $\mathcal{P}_q : \mathrm{H}_0^{-1/2}(\Gamma) \longrightarrow (\mathrm{H}_0^{-1/2}(\Gamma))^{n-1}$.

It is useful to define the following variations on $\mathrm{H}(div, \Omega)$ and $\mathrm{H}(curl, \Omega)$.

DEFINITION 3.1. *For $q \in \mathrm{L}^\infty(\Omega)$, let $\mathrm{W}_q = \mathrm{H}(div\ e^{q}, \Omega) \cap \mathrm{H}(curl\ e^{-q}, \Omega)$, where*

$$\begin{aligned} \mathrm{H}(div\ e^{q}, \Omega) &= \{\mathbf{u} \in (\mathrm{L}^2(\Omega))^n : \nabla\cdot e^{q}\mathbf{u} \in \mathrm{L}^2(\Omega)\}\,,\\ \mathrm{H}(curl\ e^{-q}, \Omega) &= \left\{\mathbf{u} \in (\mathrm{L}^2(\Omega))^n : \nabla\times e^{-q}\mathbf{u} \in (\mathrm{L}^2(\Omega))^{2n-3}\right\}, \end{aligned}$$

for $n = 2, 3$. Also, in the FOSLS setting, if $\mathbf{u}$ solves (3.1) with boundary data h, then we refer to $\{\mathbf{u}, h, \mathcal{P}_{q^*}(h)\}$ as a normal-tangential triple (NT triple) for q and to $\{h, \mathcal{P}_{q^*}(h)\}$ as an NT pair.

Given the boundary data, $\{h_i, \mathcal{P}_{q^*}(h_i)\}_{i=1}^{L}$, associated with an unknown q^* we approximate q^* by minimizing the FOSLS functional

$$\mathcal{F}_{OSLS}(q; \{h_i, \mathcal{P}_{q^*}(h_i)\}_{i=1}^{L}) = \sum_{i=1}^{L}\left(\min_{\mathbf{u}_i \in \mathrm{W}_q} \mathrm{F}(q, \mathbf{u}_i; h_i, \mathcal{P}_{q^*}(h_i))\right), \tag{3.2}$$

where

$$\mathrm{F}(q, \mathbf{u}_i; h_i, \mathcal{P}_{q^*}(h_i)) := \|e^{-q}\nabla \cdot e^q \mathbf{u}_i\|^2_{0,\Omega} + \|e^q \nabla \times e^{-q}\mathbf{u}_i\|^2_{0,\Omega} + \|\mathbf{n}\cdot e^q\mathbf{u}_i - h_i\|^2_{-1/2,\Gamma} + \|\mathbf{n}\times e^{-q}\mathbf{u}_i - \mathcal{P}_{q^*}(h_i)\|^2_{-1/2,\Gamma} . \tag{3.3}$$

To minimize $\mathcal{F}_{OSLS}$, first note that, for fixed approximation q, each $\mathbf{u}_i$ can be solved with optimal efficiency [3]. Furthermore, if we assume $q \in \mathrm{H}^1(\Omega)$ and $\mathbf{u} \in \mathrm{W}_0 = \mathrm{H}(div, \Omega) \cap \mathrm{H}(curl, \Omega)$, then for fixed $\mathbf{u}_i \in (\mathrm{H}^1(\Omega))^n$, we also have an elliptic problem to improve approximation $q \in \mathrm{H}^1(\Omega)$. Taking the first variation in q of $\mathcal{F}_{OSLS}$ for a fixed set, $\{\mathbf{u}_i \in (\mathrm{H}^1(\Omega))^2\}$, reveals that the best $q \in \mathrm{H}^1(\Omega)$ satisfies the weak form

$$\langle A\nabla q, \nabla r\rangle_{0,\Omega} = f(r) \qquad \forall\, r \in \mathrm{H}^1(\Omega)\,, \tag{3.4}$$

where

$$A = 2\sum_{i=1}^{L} |\mathbf{u}_i|^2 \tag{3.5}$$

and $f \in \mathrm{H}^{-1}(\Omega)$, for $n = 2$, is given by

$$\langle f, r\rangle_{0,\Omega} = \sum_{i=1}^{L} \left(\langle \nabla\cdot\mathbf{u}_i, \nabla r\cdot\mathbf{u}_i\rangle_{0,\Omega} + \langle \nabla\times\mathbf{u}_i, \nabla^{\perp} r\cdot\mathbf{u}_i\rangle_{0,\Omega}\right)\,,$$

using $(\boldsymbol{\tau}\cdot)$ in lieu of $(\mathbf{n}\times)$ and $(\nabla^{\perp}\cdot)$ in lieu of $(\nabla\times)$. These properties suggest that we can employ an alternating subspace minimization scheme. Before stating this iteration, we remark that the minimization associated with the weak form in (3.4) incorporates a weighting on the components of q that is directly related to the natural norm defined in (2.6) since $\mathbf{u} = \sigma^{1/2}\nabla p$. Granted, the assumption that $q \in \mathrm{H}^1(\Omega)$ is quite restrictive. For this reason, the OLS or Kohn and Vogelius approach may be better suited for many applications. However, the role of FOSLS as a framework for EIT is compelling, and its exploration is warranted out of theoretical concern alone.

3.2. Alternating Subspace Iteration. The FOSLS formulation suggests the following algorithm.

ALGORITHM 1 (Alternating Subspace Iteration (ASI)). *One sweep of this scheme is defined by the following two steps:*

1. *With conductivity* e^{2q} *fixed, approximate* $\mathbf{u}_i \in \mathrm{W}_q$ *for each Normal-Tangential (NT) pair of boundary data,* $\{h_i, \mathcal{P}_{q^*}(h_i)\}$ *for* $i = 1, \ldots, L$*, by finding the* arg min *in the finite element space* $\mathrm{W}^h_q \in \mathrm{W}_q$

$$\min_{\mathbf{u}_i \,\in\, \mathrm{W}^h_q} \mathrm{F}(q, \mathbf{u}_i; h_i, \mathcal{P}_{q^*}(h_i))\,, \tag{3.6}$$

where

$$\mathrm{F}(q, \mathbf{u}_i; h_i, \mathcal{P}_{q^*}(h_i)) := \|e^{-q}\nabla \cdot e^q \mathbf{u}_i\|^2_{0,\Omega} + \|e^q \nabla^{\perp} \cdot e^{-q}\mathbf{u}_i\|^2_{0,\Omega} + \|\mathbf{n}\cdot e^q\mathbf{u}_i - h_i\|^2_{-1/2,\Gamma} + \|\boldsymbol{\tau}\cdot e^{-q}\mathbf{u}_i - \mathcal{P}_{q^*}(h_i)\|^2_{-1/2,\Gamma} .$$

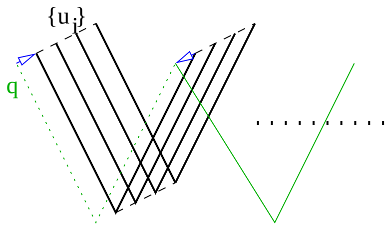

FIG. 3.1. *Alternating Subspace Iteration.*

2. *With currents* $\{\mathbf{u}_i\}_{i=1}^L$ *fixed, find* $q \in \mathrm{H}^1(\Omega)$ *such that* $q_{|\Gamma} = q^*_{|\Gamma}$ *by solving the weak form*

$$\langle A\nabla q, \nabla r\rangle_{0,\Omega} = f(r) \qquad \forall\, r \in \mathrm{H}^1(\Omega), \tag{3.7}$$

where

$$A = 2\sum_{i=1}^{L} |\mathbf{u}_i|^2$$

and

$$f(r) = \sum_{i=1}^{L} \left(\langle \nabla\cdot\mathbf{u}_i, \nabla r\cdot\mathbf{u}_i\rangle_{0,\Omega} + \langle \nabla\times\mathbf{u}_i, \nabla^{\perp} r\cdot\mathbf{u}_i\rangle_{0,\Omega}\right).$$

In Figure 3.1, we depict the multigrid V-cycles to be performed at each iteration of ASI. The black V-cycles represent application to forward problems (3.6) for each current $\{\mathbf{u}_i\}_{i=1}^L$, while the green V-cycle refers to elliptic problem (3.7) for updating the approximate conductivity. The directed blue connections represent the use of the current conductivity approximation, q, in (3.6), as well as the formation of A in (3.7) from the set of currents, $\{\mathbf{u}_i\}_{i=1}^L$. Note that the respective spatial discretizations for conductivity and current are not directly tied. In the following examples, we use piecewise bilinear finite elements on a uniform grid for all quantities $\{\mathbf{u}_i\}_{i=1}^L$ and q. Before presenting these results and their analysis, we wish to emphasize the appearance of the elliptic problem in the second part of the iterative scheme.

The σ-uniformity of the above graded grids is in direct analogy to refinement in regions according to the minimization of an energy functional with mixed coefficients. It is remarkable that the alternating subspace iteration for the FOSLS functional involves, at each update of the approximate conductivity, an elliptic minimization problem with a coefficient that indeed reflects the lack of resolution away from the boundary. When currents $\mathbf{u}_i$ associated with σ closely approximate unknown currents $\mathbf{u}_i^*$ associated with σ^*, the solution of linear system (3.7) is closely related to the minimization of $\|A\nabla(q-q^*)\|^2$, where $A = A(\{\mathbf{u}_i^*\})$. Given the use of the H^1-norm as a regularization term in OLS, there may be a tendency to liken the FOSLS approach to a more natural H^1-norm penalty on the approximate conductivity, one that better incorporates the physics. However, the H^1-norm penalty term used as a standard regularization for OLS serves to smooth the approximate conductivity, irrespective of location in the domain. The FOSLS approach, in contrast, smoothes the *error* associated with the approximation, and does so relative to distance from the boundary. The FOSLS minimization principle is therefore more closely aligned with the nature of the physics when compared to a generic regularization process.

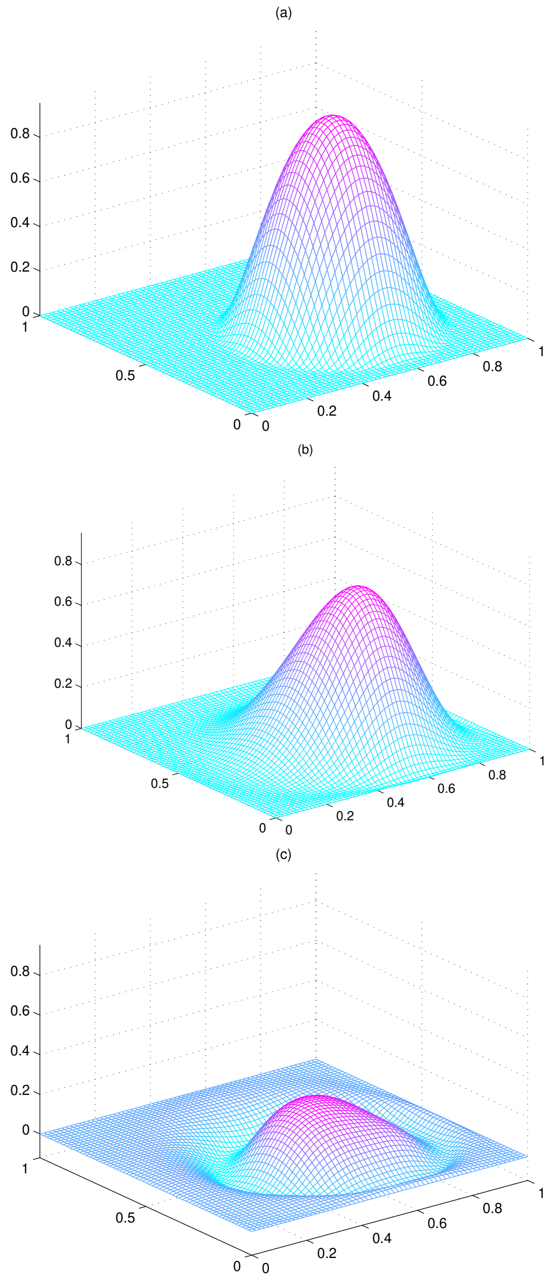

FIG. 3.2. *(a) Exact q^*, (b) approximate q, and (c) associated error $q^* - q$.*

3.3. Examples.

3.3.1. Example 1. Consider a unit square domain with exact q^* as pictured in Figure 3.2 (a), corresponding to the exact σ^* in Figure 3.3 (a). For the boundary data associated with q^*, we impose normal currents $h_i \in \{\sin(kt\pi/2), \cos(kt\pi/2)\}_{k=1}^{4}$, where $t \in [0, 4]$ is the arc length parametrization of our square. For each $\mathbf{u}_i$ subject

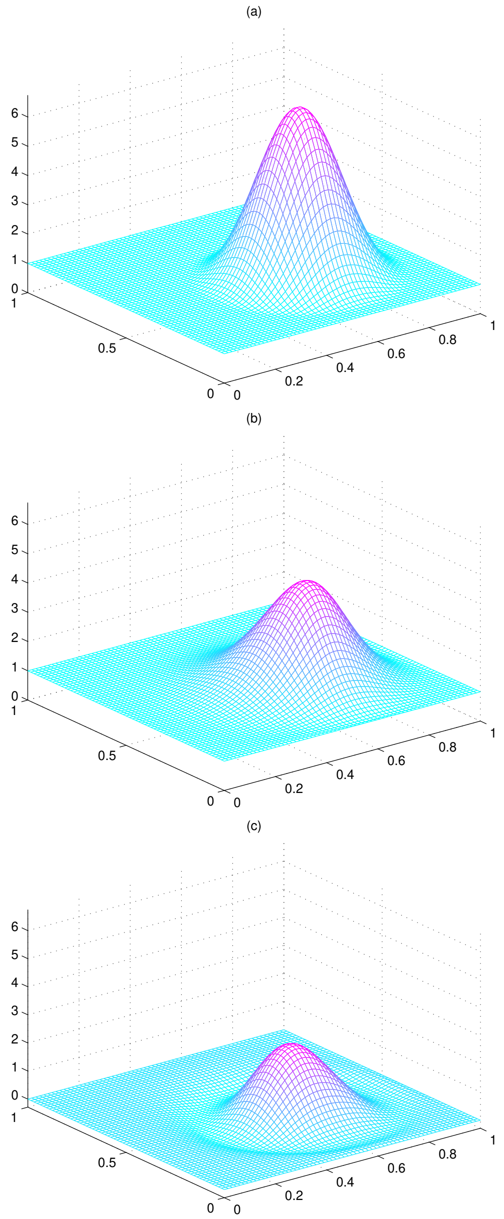

FIG. 3.3. *(a) Exact σ^* , (b) approximate σ, and (c) associated error $\sigma^* - \sigma$.*

to h_i, we compute

$$\min_{\mathbf{u}_i \,\epsilon\, \mathrm{W}^h_{q^*}} \left\{ \|e^{-q^*}\nabla \cdot e^{q^*}\mathbf{u}_i\|^2_{0,\Omega} + \|e^{q^*}\nabla^{\perp} \cdot e^{-q^*}\mathbf{u}_i\|^2_{0,\Omega} \right\}$$

and read the tangential data, $\tau \cdot e^{-q^*}\mathbf{u}_i =: \mathcal{P}^h_{q^*}(h_i)$. Hence, the measured data is simulated according to a discrete Normal-to-Tangential (NtT) map. Given this data, and using $q_0 = 0$ as an initial guess, we perform 15 iterations of our algorithm. All computation is done on a 64×64-grid, so that $h = 1/64$.

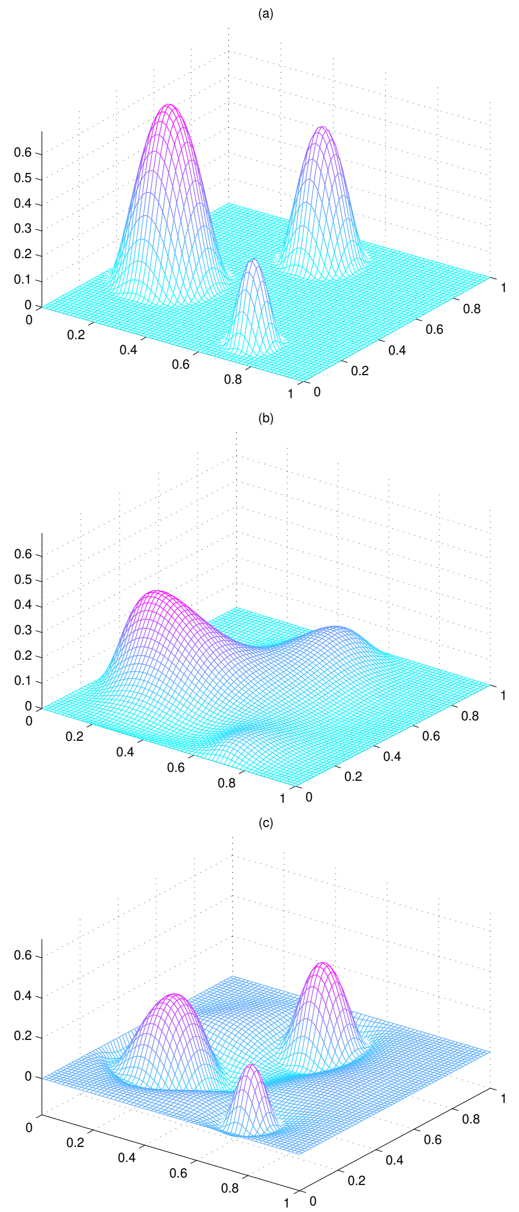

FIG. 3.4. *(a) Exact q^*, (b) approximate q, and (c) associated error $q^* - q$.*

In Figure 3.2, we plot q^*, q, and their difference. Figure 3.3 is analogous, but in conductivities $\sigma^* = e^{2q^*}$ and $\sigma = e^{2q}$. Observe that the L^∞-norm of the error is roughly 25%, but that the postion of the inhomogeneity is accurate. Before discussing this reconstruction further, we present an example with three isolated inhomogeneities.

3.3.2. Example 2. As above, we compute the discrete NtT map corresponding to q^* in Figure 3.4. The associated σ^* is in Figure 3.5. We use the same imposed boundary currents as in the above example and, again, all computation is done on a

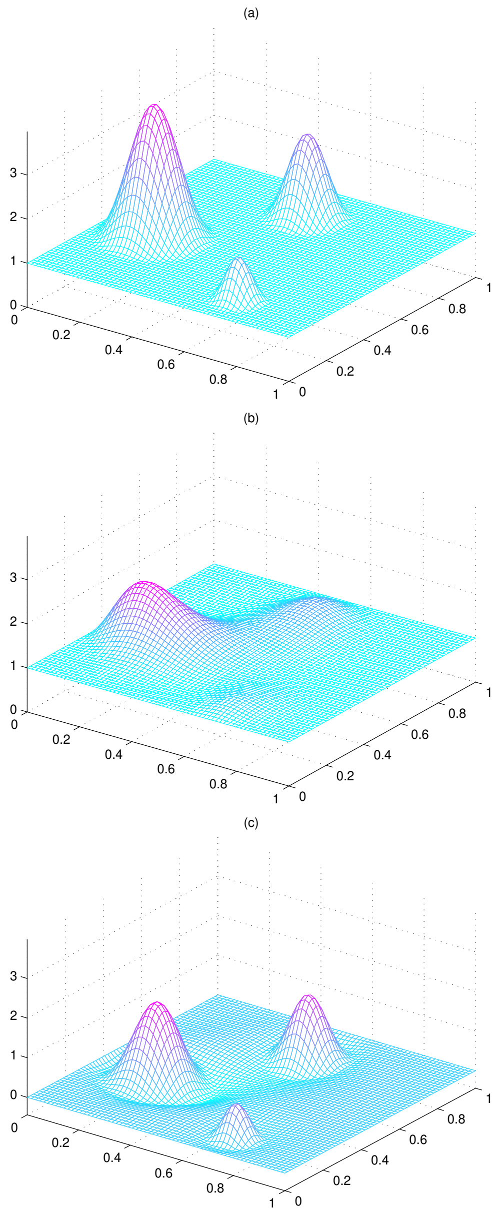

FIG. 3.5. *(a) Exact σ^* , (b) approximate σ, and (c) associated error $\sigma^* - \sigma$.*

uniform grid with $h = 1/64$.

We plot q^*, q, and their difference in Figure 3.4 and similarly for conductivity in Figure 3.5. Immediately, one observes that the error, when measured in a conventional sense, is quite large.However, again the resolution nearest the boundary does indicate the position of the three isolated inhomogeneities. In the next section, we confirm that the computable lower bound, established in the previous chapter, holds in each example; that is, that the error in each example is small in our measure.

3.4. Analysis. In the following, we demonstrate computation of the lower bound established in the previous section, and verify that the estimates hold for each of the above examples. Recall that $h^* \in \mathrm{H}_0^{-1/2}(\Gamma)$ is defined so that

$$\|\mathcal{R}_\sigma(h^*) - \mathcal{R}_{\sigma^*}(h^*)\|_{1/2,\Gamma} = \|\mathcal{R}_\sigma - \mathcal{R}_{\sigma^*}\|_{\mathcal{L}(\mathrm{H}_0^{-1/2}(\Gamma),\mathrm{H}_0^{1/2}(\Gamma))}\,.$$

Let ϕ be any element of $\mathcal{T}$, the space of available normal imposed currents. Combining Theorem 2.4 with the result of Lemma 2.3.1, we have

$$\begin{aligned}\|\mathcal{P}_q(\phi) - \mathcal{P}_{q^*}(\phi)\|_{-1/2,\Gamma} &+ c\|h^* - \phi\|_{-1/2,\Gamma} \\ &\geq (\min_\Omega 1/\eta) \sup_{\psi_1,\psi_2\in\mathcal{T}} \frac{\left|\int_\Omega (\sigma - \sigma^*)\,\nabla p_1 \cdot \nabla p_2\,dx\right|}{\|\psi_1\|_{-1/2,\Gamma}\|\psi_2\|_{-1/2,\Gamma}}\,,\end{aligned} \tag{3.8}$$

where the sup is taken over all DN triples, $\{p_1, \mathcal{R}_\sigma(\psi_1), \psi_1\}$ and $\{p_2, \mathcal{R}_\sigma(\psi_2), \psi_2\}$, and where $c = 2\max\{\|\mathcal{R}_\sigma\|_{\mathcal{L}}, \|\mathcal{R}_{\sigma^*}\|_{\mathcal{L}}\}$.

To check whether our numerical results are faithful to (3.8), we find estimates for each of the relevant quantities. To this end, we appeal to the Fourier transform to compute the $\mathrm{H}^{-1/2}$-norms that appear in (3.8). For example, from [9] we have

$$\|\cos(kt\pi/2)\|_{-1/2,\Gamma} = (k\pi/2)^{-1/2}\|\cos(kt\pi/2)\|_{0,\Gamma} \tag{3.9}$$

on a circle. Though our domain is a square, we appeal to this estimate and expect that (3.9) provides a reliable approximation since our boundary is smooth almost everywhere. Using (3.9) and an analogous result for $\sin(kt\pi/2)$, we are able to form a mass matrix associated with the $\mathrm{H}^{-1/2}$-norm and a trigonometric basis, $\{\sin(kt\pi/2), \cos(kt\pi/2)\}_{k=1}^N$. For $\psi \in \mathcal{T}_{2N} := Span\{\sin(kt\pi/2), \cos(kt\pi/2)\}_{k=1}^N$, we may write

$$\|\psi\|^2_{-1/2,\Gamma} = \beta^t M\beta\,, \tag{3.10}$$

where β is the vector of coefficients in our trigonometric basis and

$$M = \begin{pmatrix} \ddots & & & \\ & \frac{2}{k\pi}\|\cos(kt\pi/2)\|^2_{0,\Gamma} & & \\ & & \frac{2}{k\pi}\|\sin(kt\pi/2)\|^2_{0,\Gamma} & \\ & & & \ddots \end{pmatrix} \tag{3.11}$$

is an $2N \times 2N$ diagonal matrix.

To begin assessing each of the terms on the left side of (3.8), we must approximate h^* and choose $\phi \in \mathcal{T}$. As our only option, we estimate h^* by expanding the space of imposed currents; here, given that $\phi \in \mathcal{T}_8 := Span\{\sin(kt\pi/2), \cos(kt\pi/2)\}_{k=1}^4$ for our examples, we expand the space to $\mathcal{T}_{20} := Span\{\sin(kt\pi/2), \cos(kt\pi/2)\}_{k=1}^{10}$. We choose the approximate h^* so that

$$\begin{aligned}\frac{\|\mathcal{P}_q(h^*) - \mathcal{P}_{q^*}(h^*)\|_{-1/2,\Gamma}}{\|h^*\|_{-1/2,\Gamma}} &= \sup_{\psi\in\mathcal{T}_{20}} \frac{\|\mathcal{P}_q(\psi) - \mathcal{P}_{q^*}(\psi)\|_{-1/2,\Gamma}}{\|\psi\|_{-1/2,\Gamma}} \\ &= \sup_{\psi_1,\psi_2\in\mathcal{T}_{20}} \frac{\langle\psi_1, \mathcal{P}_q(\psi_2) - \mathcal{P}_{q^*}(\psi_2)\rangle_{0,\Gamma}}{\|\psi_1\|_{-1/2,\Gamma}\|\psi_2\|_{-1/2,\Gamma}}\,.\end{aligned} \tag{3.12}$$

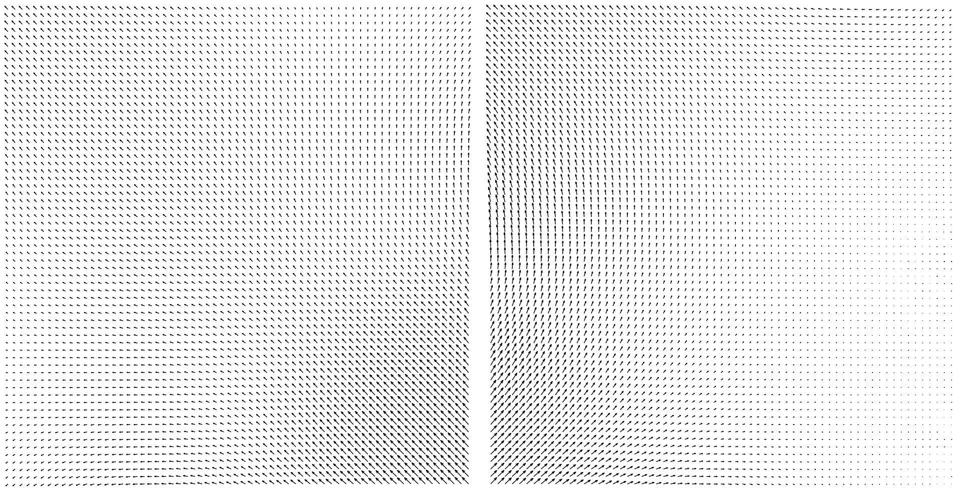

FIG. 3.6. *"Best test" for examples 1 (left) and 2. Note that, for example 1, the single inhomogeneity is located in the bottom right where the current is focused. Similarly, the best test for example 2 focuses on the left side of the domain, the location of the most significant of the three inhomogeneities.*

There are now several options for choosing ϕ, since our theorem only assumes that it belongs to the span of available tests. As a first option, we could find ϕ such that

$$\|h^* - \phi\|_{-1/2,\Gamma} = \min_{\psi \in \mathcal{T}_8} \|h^* - \psi\|_{-1/2,\Gamma} .$$

An alternative candidate for $\phi \in \mathcal{T}$ is that which achieves the sup in the lower bound in (3.8). However, perhaps the most effective choice is to consider ϕ in analogy to (3.12): define ϕ such that

$$\frac{\|\mathcal{P}_q(\phi) - \mathcal{P}_{q^*}(\phi)\|_{-1/2,\Gamma}}{\|\phi\|_{-1/2,\Gamma}} = \sup_{\psi_1,\psi_2 \in \mathcal{T}_8} \frac{\langle \psi_1, \mathcal{P}_q(\psi_2) - \mathcal{P}_{q^*}(\psi_2)\rangle_{0,\Gamma}}{\|\psi_1\|_{-1/2,\Gamma}\|\psi_2\|_{-1/2,\Gamma}} . \tag{3.13}$$

Since we have $\phi = \sum \beta_i h_i$, where $h \in \{\sin(kt\pi/2), \cos(kt\pi/2)\}_{k=1}^{4}$, we may use (3.10) and (3.11) and compute β as the 8×1 singular vector associated with the sup achieved in (3.13). We have chosen ϕ according to (3.13) to demonstrate the theory and compute estimates of the terms that appear in (3.8). In Figure 3.6, we display ϕ associated with Example 1 and Example 2.

The importance of this choice for ϕ is that it can be conducted without knowledge of q^*, since it only depends on the given and computed boundary data. This suggests the use of adaptive testing to reduce the number of forward problems computed at each iteration, a concept introduced in [7]. In each of the above three choices, test ϕ is, in a closely related sense, the best way to signal the error, $q - q^*$, when restricted to boundary tests in $\mathcal{T}_8$.

To estimate the first term in the upper bound in (3.8), we must account for only being able to compute a discrete NtT map, which we denote $\mathcal{P}_q^h$. Analogous to our approximation of h^*, we appeal to $\mathcal{P}_q^{h/8}$ to represent the "continuous" NtT map.

Terms for (3.8)	Example 1	Example 2
$\|\mathcal{P}_q^h(\phi) - \mathcal{P}_{q^*}^h(\phi)\|_{-1/2,\Gamma}$	2.3×10^{-5}	6.1×10^{-5}
$\|\mathcal{P}_q^{h/8}(\phi) - \mathcal{P}_q^h(\phi)\|_{-1/2,\Gamma}$	2.7×10^{-4}	3.4×10^{-4}
$\|\mathcal{P}_{q^*}^{h/8}(\phi) - \mathcal{P}_{q^*}^h(\phi)\|_{-1/2,\Gamma}$	3.1×10^{-4}	8.5×10^{-4}
$c\|h^* - \phi\|_{-1/2,\Gamma}$	.1916	.5849
$s_{max}(\sigma)$	.01668	.01155

TABLE 3.1
Estimated terms confirming that inequality (3.8) holds.

Introducing these quantities and using the triangle inequality, we have

$$\begin{aligned} &\|\mathcal{P}_q(\phi) - \mathcal{P}_{q^*}(\phi)\|_{-1/2,\Gamma} \\ &\quad \leq \|\mathcal{P}_q^h(\phi) - \mathcal{P}_{q^*}^h(\phi)\|_{-1/2,\Gamma} + \|\mathcal{P}_q(\phi) - \mathcal{P}_q^h(\phi)\|_{-1/2,\Gamma} + \|\mathcal{P}_{q^*}(\phi) - \mathcal{P}_{q^*}^h(\phi)\|_{-1/2,\Gamma} \\ &\quad \approx \|\mathcal{P}_q^h(\phi) - \mathcal{P}_{q^*}^h(\phi)\|_{-1/2,\Gamma} + \|\mathcal{P}_q^{h/8}(\phi) - \mathcal{P}_q^h(\phi)\|_{-1/2,\Gamma} + \|\mathcal{P}_{q^*}^{h/8}(\phi) - \mathcal{P}_{q^*}^h(\phi)\|_{-1/2,\Gamma} \,. \end{aligned} \tag{3.14}$$

The first term in (3.14) represents the effectiveness of our FOSLS functional minimization. In [10], we related the first term through a series of constants to the value of the FOSLS functional. However, rather than trace through those constants here, we simply compute

$$\|\mathcal{P}_q^h(\phi) - \mathcal{P}_{q^*}^h(\phi)\|_{-1/2,\Gamma}$$

according the the results of the FOSLS minimization for each example. Again, we compute in the $\mathrm{H}^{-1/2}$-norm using a trigonometric basis and appeal to (3.10) and (3.11); hence, this estimate is rough in that our domain is a square and that the boundary data is piecewise linear. Nonetheless, we believe that it is telling. The resulting estimates for each example are listed Table 3.1. Similarly, we approximate the second and third terms in (3.14), which represent the accuracy of the discrete NtT maps associated, respectively, with q and q^*. However, this computation is done on the fine grid having interpolated the data up to the $h/8$ grid. For $h = 1/64$, we have the values listed in Table 3.1.

The final term in the inequality, $c\|h^* - \phi\|_{-1/2,\Gamma}$, represents our ability to signal the error given our limited space of applied tests, $\mathcal{T}_8$. Table 3.1 contains estimate of this term. We estimate $c = 2\max\{\|\mathcal{P}_q\|_{\mathcal{L}}, \|\mathcal{P}_{q^*}\|_{\mathcal{L}}\}$ to find $c = 2.8$ and $c = 8.4$ in Examples 1 and 2, respectively. This suggests that we are performing the minimization of our FOSLS functional sufficiently well and that, in order to improve the estimates, enhancing the testing capacity is imperative to overcome the precision lost in the series of inequalities. We also remark that the use of sines and cosines toward a basis of $\mathrm{H}^{-1/2}$ facilitates the analysis, but it is lacking in the sense that higher frequency modes contribute exponentially less insight on the interior. To introduce an

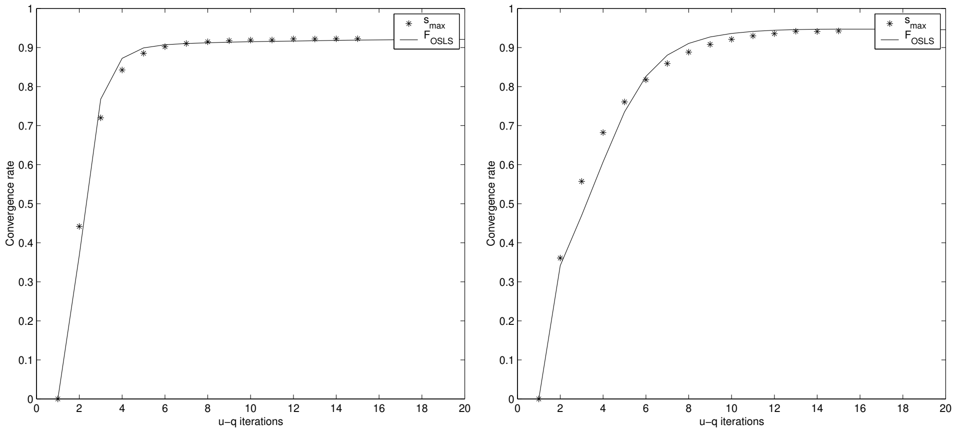

FIG. 3.7. *Convergence factors for examples one and two. For clarity, the data for the FOSLS factor is connected by a solid line.*

array of compactly supported tests will require consistency in the bounds and thus computation of the $\mathrm{H}^{-1/2}$-norm.

Finally, we estimate the lower bound in (3.8). Writing (3.11) enables us to compute the lower bound as the maximum singular value of, in this case, an 8×8 matrix. We define

$$s_{max}(\sigma) := (\min_{\Omega} 1/\eta) \sup_{\psi_1, \psi_2 \in \mathcal{T}_8} \frac{\left| \int_\Omega (\sigma - \sigma^*) \nabla p_1 \cdot \nabla p_2 \, dx \right|}{\|\psi_1\|_{-1/2,\Gamma} \|\psi_2\|_{-1/2,\Gamma}}, \tag{3.15}$$

and observe the values in Table 3.1, where σ is the approximation after 15 iterations for each example. Clearly, (3.8) holds in each example. The disparity in terms suggests that our FOSLS minimization is sufficient, and that more emphasis should be placed on generating especially revealing boundary data. However, one should note that better data is likely to only improve the resolution that can be obtained near the boundary.

Having established the faithfulness of our numerical results, we remark on the convergence of our basic algorithm. Figure 3.7 compares convergence factors for the FOSLS functional to the convergence factors for our lower bound, $s_{max}(\sigma)$. We recall that the lower bound depends on the existing approximation. Denoting the ith approximate conductivity as σ_i, we compute and plot the quantities

$$\rho_s^i = \frac{s_{max}(\sigma_{50}) - s_{max}(\sigma_i)}{s_{max}(\sigma_{50}) - s_{max}(\sigma_{i-1})} \tag{3.16}$$

and

$$\rho_{FOSLS}^i = \frac{\mathcal{F}_{OSLS}(\sigma_{50}) - \mathcal{F}_{OSLS}(\sigma_i)}{\mathcal{F}_{OSLS}(\sigma_{50}) - \mathcal{F}_{OSLS}(\sigma_{i-1})} \tag{3.17}$$

for $i = 1, \ldots, 15$. The aligned convergence factors appear to be bounded below 1, suggesting the conjecture that the angle between the subspaces for q and $\{\mathbf{u}_i\}_{i=1}^L$ is uniformly positive. The implication is that ASI converges, with factor $\rho_{FOSLS}^i \approx .9$, in the natural norm on error in conductivity. Thet the two convergence factors differ is unfortunate but perhaps not surprising given the inherent dependence of the problem on the true conductivity to be resolved.

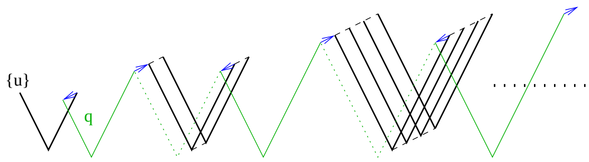

FIG. 4.1. *Improved algorithm.*

4. Conclusions.

4.1. Towards an improved algorithm. In Figure 4.1, several improvements on the basic alternating subspace iteration are visualized. One major priority is reducing the number of minimizations for the set, $\{\mathbf{u}_i\}_{i=1}^{L}$, used in each update for q. If there is no structural a priori information available, we suggest building the approximate q in the interior first, using slowly varying boundary data. Then, one can incorporate additional high frequency data into the determination of the next approximation for q. This is analogous to the concept of layer-stripping [15] and in line with the recent approach of Borcea [2] for Output Least Squares. In Figure 4.1, we portray beginning on a coarse level for q and adding tests as the iterative method progresses.

A viable option for focusing and accumulating the boundary data used in the first step of the alternating subspace iteration is to first compute many currents associated with an initial guess. Next, we would determine the ϕ that plays the role in our theory, as well as the next few singular vectors corresponding to the largest singular values. These few tests can then be used to target the existing error efficiently, significantly reducing the number of forward problems at each iteration. This process can then be repeated once the approximation changes significantly.

Additionally, one should perform the interior updates of q using a coarse grid representation of the computed $\{\mathbf{u}_i\}_{i=1}^{L}$. The dashed V-cycles [16] in Figure 4.1 are to highlight that the nonlinear connection, between q and $\{\mathbf{u}_i\}_{i=1}^{L}$, is realizable in the multigrid setting; i.e., updates can be performed entirely within a given grid level. This offers a natural and efficient way to update q in the interior, avoiding excessive computation to determine the fine grid current at each iteration.

There is evidently a wealth of directions for future research. However, while the above suggestions should certainly improve the efficiency of our FOSLS minimization, it is not realistic to think that they will significantly improve the reconstruction of an unknown conductivity. For the latter, we are at the mercy of the physics and the incomplete data, as our theory suggests.

4.2. Final Summary. The theory herein represents an advance in understanding the inverse problem of EIT. Moreover, the equivalence of three least-squares approaches proved in [10] forms a framework encompassed by this theory. Within the most general spaces according to Sobolev and without appealing to linearization, we quantified and observed how the pre-imposed discreteness and inexactness of finite data combine to render classes of internal conductivity indistinguishable. Though we do not avoid deterioration of our bounds in the event that conductivity varies in a given domain by orders of magnitude, the technique we use to address the nonlinear problem may be refined.

When little a priori information is available, we give examples of how the theory can be used to guide a discretization of conductivity that uniformly distributes the uncertainty with which conductivities can be distinguished. Given problem specific information that admits a basis for conductivity catered to the computational objective, the theory similarly quantifies what may be rightfully reconstructed from a particular set of boundary data. Finally, our theory expresses the implications of finite boundary data in the most general Sobolev boundary spaces. Each of these contributions entreat future research, especially in the context of additional problem specific information, where the flexibility of the variational setting becomes crucial.

We claim that our theory establishes the core of an optimal multilevel reconstruction algorithm that incorporates the intrinsic loss of resolution due not only to the physics, but also to the inexact and finite set of available boundary data. This claim is not yet substantiated by numerical results for the FOSLS formulation. However, the theory and preliminary results of these papers suggest a new and potentially powerful approach to the EIT problem.

REFERENCES

[1] G. Alessandrini, *Singular solutions of elliptic equations and the determination of conductivity by boundary measurements*, Journal of Differential Equations, 84 (1990), pp. 252–272.

[2] L. Borcea, *A nonlinear multigrid for imaging conductivity and permittivity at low frequency*, Inverse Problems, 17 (2001), pp. 329–360.

[3] Z. Cai, T. Manteuffel, and S. McCormick, *First-order system least squares for second-order partial differential equations: Part II*, SIAM Journal On Numerical Analysis, 34 (1997), pp. 425–454.

[4] A. Calderon, *On an inverse boundary problem*, in Seminar on Numerical Analysis and its Applications to Continuum Physics, W. Meyer and M. Raupp, eds., Rio de Janeiro, 1980, Brazilian Math. Society, pp. 65–73.

[5] M. Cheney and D. Issacson, *Distinguishability in impedance imaging*, IEEE Transactions on biomedical engineering, 39 (1992), pp. 852–860.

[6] A. Friedman, *Introduction to Modern Analysis*, Dover Publications, Inc., New York, 1982.

[7] D. Gisser, D. Isaacson, and J. Newell, *Electric current computed tomography and eigenvalues*, SIAM Journal of Applied Mathematics, 50 (1990), pp. 1623–1634.

[8] D. Isaacson, *Distinguishability of conductivities by electric current computed tomography*, IEEE Transactions On Medical Imaging, 5 (1986), pp. 91–95.

[9] J. L. Lions and E. Magenes, *Non-Homogeneous Boundary Value Problems and Applications*, Springer-Verlag, Berlin, 1972.

[10] H. MacMillan, S. McCormick, and T. Manteuffel, *First-order system least squares and electrical impedance tomography: Part I.* Submitted.

[11] R. L. Parker, *The inverse problem of electrical conductivity in the mantle*, Geophysical Journal of the Royal Astronomical Society, 22 (1970), pp. 121–138.

[12] ———, *Geophysical Inverse Theory*, Princeton Universty Press, Princeton, N.J., 1996.

[13] A. Seagar, T. Yeo, and R. Bates, *Full-wave computed tomography: resolution limits*, IEE Proceedings, Pt. A, Physical Science and Measurement, 131 (1984), pp. 616–622.

[14] A. D. Seagar, T. S. Yeo, and R. H. Bates, *Full-wave computed tomography:low frequency electric current*, IEE Proceedings, Pt. A, Physical Science and Measurement, 132 (1985), pp. 455–466.

[15] E. Somersalo, M. Cheney, D. Isaacson, and E. Isaacson, *Layer stripping: A direct numerical method for impedance imaging*, Inverse Problems, 7 (1991), pp. 899–926.

[16] U. Trottenberg, C. Oosterlee, and A. Schuller, *Multigrid*, Academic Press, London, 2001.